J. of Supercritical Fluids 112 (2016) 103–113

Contents lists available at ScienceDirect

The Journal of Supercritical Fluids

journal homepage: www.elsevier.com/locate/supflu

Molecular dynamics simulation study: The reactivation of NaX zeolite contaminated by bi and tri aromatics using supercritical fluid extraction

M. Haghighi Asl [a], F. Moosavi [b], J. Sargolzaei [a,*]

[a] Department of Chemical Engineering, Ferdowsi University of Mashhad, PO Box 9177948944, Mashhad, Iran
[b] Department of Chemistry, Ferdowsi University of Mashhad, PO Box 9177948974, Mashhad, Iran

ARTICLE INFO

Article history:
Received 3 November 2015
Received in revised form 3 January 2016
Accepted 4 January 2016
Available online 3 March 2016

Keywords:
Supercritical fluid extraction
NaX zeolites
Naphthalene
Anthracene
Carbon dioxide

ABSTRACT

In the present work, the supercritical fluid extraction (SFE) process was utilized to reactivate deactivated NaX zeolite with bi and tri aromatic contaminants (naphthalene and anthracene). In this direction, different parameters including extraction static time (30–120 min), extraction pressure (80–350 bar), extraction temperature (323.15–373.15 K) and using two common and polar modifiers, methanol and dichloromethane, were investigated. The obtained results show that the optimum parameters were extraction pressure and temperature of 350 bar and 373.15, respectively as well as static time of 90 min to have the highest extraction value. However, modifiers did not display any significant influence on extraction efficiency. In addition, molecular dynamics simulations have been carried out to provide an atomic description of the supercritical carbon dioxide behavior with contaminants trapped inside NaX zeolite. The force field parameters were chosen carefully to examine self-diffusion coefficient of sorbates over a wide range of loading, temperature, and pressure. The simulated self-diffusivity was found to be in a reasonable agreement with the corresponding experimental data which evaluate the effectiveness of proposed calculation method and force field accuracy. All involved calculations were performed in time period 6 ns and repeated calculations have been done at least two times to confirm the results and applied average values, which made the results being reliable.

1. Introduction

Zeolite deactivation, the loss over time of activity and/or selectivity, is a problem of great and continuing concern in the practice of industrial adsorption processes. Cost to industry for zeolite replacement and process shuts down billions of dollars per year. Zeolites are crystalline aluminosilicates with micropores of uniform size extensively used in adsorption applications [1–6]. These materials may possess variety of framework structures originated from distinct microporous structures. The size and shape of the zeolite micropores are tremendously important for adsorption considering the organic compounds as adsorbates have molecular sizes similar to the pore dimension [7]. Literature survey demonstrates that slight variations in the size of the pores as well as surface chemical composition impact drastically on the performance of zeolitic materials as adsorbents and molecular sieves [1,8–18]. Based on the aforementioned statements, deactivation of zeolite is an unfavorable phenomenon. In this direction, there are two main approaches including zeolite replacement along activation and regeneration of the deactivated zeolite to enhance the efficiency of the adsorption process. As a result, zeolite replacement leads to huge amount of investments. In other words, activation and regeneration of the deactivated zeolite seems to be more economic compared to replacement of deactivated zeolite with fresh one [19].

Supercritical fluid extraction (SFE) has proven to be a valuable alternative method of extraction. SFE results in a dramatic decrease in extraction times and avoids the use of large quantities of organic solvents that are often toxic. Given the difficulties in experimentally obtaining accurate and reproducible SFE phenomenon, molecular dynamics (MD) simulation methods have been shown to be particularly powerful to study SFE in zeolites [20].

* Corresponding author. Tel.: +98 915 512 4591; fax: +98 511 762 81 03.
E-mail address: sargolzaei@um.ac.ir (J. Sargolzaei).

http://dx.doi.org/10.1016/j.supflu.2016.01.003
0896-8446/

Atomic models and algorithms allow accurate calculations and behavior decryption of different systems. MD is the most common method to carry out simulations for considering unknown behavior in porous adsorbents [21]. It is, therefore, interesting to investigate the extraction of contaminants (aromatic hydrocarbons in this paper) within the micropores of such aluminosilicate zeolites by SFE. Diffusion of molecules can be studied experimentally; however, details of the diffusion process are very difficult to be achieved by experiments. Atomistic MD simulations based on analytical potential functions provide an appropriate way to study the microscopic details of such processes as well as being effective in modeling the diffusion of organic molecules in zeolites [9,10,22,23]. Considering these various important points on adsorption, the present study focuses on the extraction of naphthalene and anthracene in NaX zeolite by supercritical carbon dioxide. However, the adsorption, diffusion, and desorption of guest molecules in zeolitic hosts are complicated and therefore it is, in general, very difficult to interpret microscopic and dynamical diffusion and desorption processes by experimental data only. So in this regard MD computer simulation can provide a powerful complimentary approach to study the adsorption, diffusion, and desorption mechanisms of a variety of guest molecules in zeolites. To the best of our knowledge, though there exists numerous simulations and experimental studies on diffusion of aromatics in zeolites including faujasite [13,24–26], MD simulation of SFE of polyaromatics from NaX zeolites has never been reported.

From the other side of view, the important point to mention is that optimization of the extraction conditions is usually assessed by systematic alteration of one variable while the others are maintained constant. However, this approach is unable to determine interactions between parameters and predict extraction conditions. In this respect, experimental designs are appropriate tools for this purpose. Furthermore, these designs allow efficient testing of method robustness [27].

In our previous study [28], detailed coke features inside industrial NaX zeolites, in terms of molecular structure and some other properties have been investigated. Coking occurs during sequenced temperature and pressure swing mercaptan removal from natural gas in industrial process at operational conditions of 300 °C and 8 bar leading to NaX deactivation. Since trapped bi and tri aromatics as the representative of industrial coke compounds inside NaX zeolite, the present study reports extraction of these trapped compounds inside NaX zeolite by SFE. At the meantime, the structural and dynamical points of view as well as the thermodynamic behaviors for atomic description of SFE mechanisms is under consideration by carrying out MD simulation.

2. Experimental details

2.1. Extraction set up

Experiments on SFE were carried out in the extraction apparatus shown schematically in Fig. 1. At first, the gas (carbon dioxide and/or propane) from a cylinder was passed through a filter and then entered into a refrigerator to make it liquid. The liquid fluid was then pumped by a reciprocating oil-free water-free high pressure pump into a vertical surge tank. The surge tank dampened the pressure fluctuations produced because of pump operation. Also, at the outlet of the surge tank a digital pressure gauge in the range of 0–600 bar by a division of 1 bar was placed to control the pressure of the system easily. The pressurized fluid then entered into an extraction vessel. The surge tank and the extraction vessel were surrounded by an oven to set the temperature of system up to 200 ± 1 °C. SFE flow under desired pressure and temperature conditions upwards through a packed bed of contaminated NaX zeolite contained in the extraction vessel 316SS (L); internal diameter of 20 mm; total length of 712 mm. To avoid undesired entrainment effects, the packed bed of NaX zeolite was located in the extraction vessel between two metallic porous plates and the extra space was filled with cotton. The equilibrated solution was then expanded by a preheated fine needle valve. The extraction pressure was measured at the entrance of the extraction vessel with an accuracy of ±0.1 MPa (Wika, Model 881.14.600, UK).

In this procedure the difference between the initial and final weight of the basket is the amount of the extracted contaminations from NaX zeolite. In other words, after finishing the extraction process, the sample was re-weighted and the difference between the initial and final masses of the zeolite was considered as the amount of the extracted contamination. The mass of extracted contaminations was determined using a Sartorius BA110S Basic series balance by accuracy of 10^{-5} g.

2.2. Materials

Naphthalene and anthracene were obtained from Merk chemicals Ltd. Group (Germany). Zeolite 13X (Si/Al = 1.00) was obtained from Zeochem Chemicals Ltd. Group (Switzerland). 13X was washed with deionized water, heated in an oven for 4–5 h, and finally cooled to room temperature in desiccator. Then 10 mg of 13X loaded with 100 mg anthracene + 100 mg naphthalene dissolved in 100 mL CH_2Cl_2 and stirred overnight at room temperature. Notice that for deposits inside zeolite, it has been calimed experimentally, in our previous study [28] that CH_2Cl_2 acts as an appropriate solvent to extract the deposits. For this reason, this modifire is applied. The

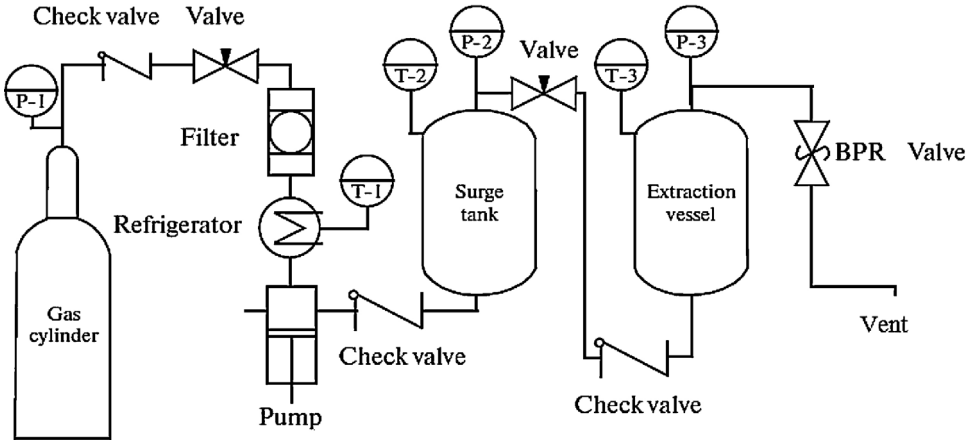

Fig. 1. High pressure apparatus for extraction of NaX zeolite contaminants.

Table 1
Physical properties of Fresh NaX zeolite.

Test	Fresh zeolite
Water adsorption capacity @ 25 °C (mass %)	
10% R. H.	19.73
20% R. H.	21.1
40% R. H.	22.8
60% R. H.	23.2
80% R. H.	25.1
BET	
Specific surface area (m^2/g)	683.91
Total pore volume @ $p/p_0 = 0.990$ (cm^3/g)	0.3725
XRD	Na_2Al_2 $Si_{2.5}$ O_9. $6.2H_2O$ (Na_2O Al_2O_3 2.5 SiO_2. 6.2 H_2O and small amount of SiO_2 quartz)

temperature of solution was increased to 70 °C in order to increase solubility of contaminants in CH_2Cl_2 and stirred overnight and then the product was treated at 270 °C for 2 h. The zeolite 13X was exchanged twice using 150 mg anthracene + 150 mg naphthalene dissolute in 50 mL methanol and 50 mL CH_2Cl_2 and again stirred overnight at room temperature. Then the product was washed with deionized water and finally heated in an oven at 100 °C for 2 h. Physical properties and elemental analysis of NaX zeolite by Energy Dispersive X-ray Spectroscopy (EDX) are given in Tables 1 and 2. Surface investigation by BET method was applied to calculate the total surface area and pore volume, two valuable paramters that are used for comparative purposes. N_2 adsorption isotherms were evaluated at −196 °C via an ASAP 2010 instrument, using N_2 of 99.99% purity. All samples were first outgassed at 305 °C for at least 3 h under vacuum.

3. MD simulation details

The structure of FAU without Na+ ectraframework cations from X-ray and neutron powder diffraction data was taken from the paper of Porcher et al. [29]. Each of two Supercages (SCs) have been connected by a 12-membered window (12-T ring) with a diameter of 7.4 Å. The framework of FAU zeolite considered here has a cubic unit cell with cell edge of $a = 24.8536$ Å. The accessible space for aromatic molecules was the SC with a diameter of ~13 Å formed by sodalite cages as shown in Fig. 2. Each unit cell contains 96 Si, 96 Al, 96 Na, and 384 O atoms with Si/Al ratio equal to one. As a result, NaX structure in a unit cell obeys the composition of $Na_{96}Si_{96}Al_{96}O_{384}$. As it is well known, the kinetic diameter is the smallest diameter that allows the adsorbate molecule to enter the inner cavity (SC in this case). Thus, the largest sorbate employed in the present study was naphthalene, which had a kinetic diameter comparable with the size of the 12-T ring.

All MD simulations were performed in NVT ensemble using Nosé-Hoover thermostat implemented by DL_POLY program package version 2.17 [30]. At the beginning of the simulations, sorbate molecules were randomly distributed around NaX surface. The simulations were performed for the loadings in the range of 1 to 8 molecules per unit cell and the highest loading of 36 molecules per unit cell was followed by the production run of 6 ns. Atomic trajectories were stored every 1000 fs for further analyses. The equations

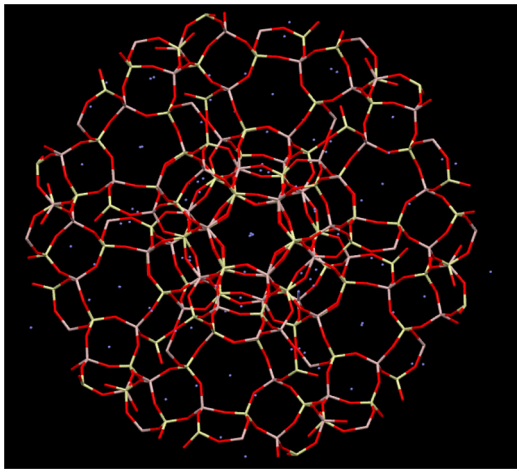

Fig. 2. Snapshots of FAU zeolite and extra framework cation distribution.

of motion were integrated by using Verlet leapfrog algorithm with a time step of 1.0 fs. Periodic boundary conditions were applied to all three dimensions. The long-range electrostatic interactions were computed using Ewald summation method and short-range van der Waals interactions were evaluated up to a cutoff radius of 12.5 Å, the half of simulation box edge.

The framework structure was built with strict alternation of the SiO_4 and AlO_4 tetrahedral shown in Fig. 2 which was fully occupied by Na^+ ions, emulated from the model described by [31,32]. The extra framework cations were allowed to move while all other framework atoms were kept fixed at the crystallographic positions during the simulations.

The total potential energy of the zeolite–sorbate complex consists of three terms in the potential function:

$$V_{total} = V_{sorbate} + V_{Zeolite} + V_{sorbate\text{-}sorbate} + V_{Zeolite\text{-}sorbate}$$

where $V_{sorbate}$ is the intramolecular potential energy of naphthalene/anthracene and carbon dioxide, $V_{zeolite}$ is the intermolecular potential energy of zeolite, $V_{sorbate-sorbate}$ is the potential energy between sorbate molecules, and $V_{zeolite-sorbate}$ is the potential energy between the naphthalene/anthracene and carbon dioxide molecules and the zeolitic atoms. The mathematical expressions used in the potential functions are shown in Supplementary materials.

The intramolecular potential energy of the sorbate molecule is taken from the work of Rungsirisakun et al. [9,33]. It consists of five terms for bond stretching, bending, and torsion as well as van der Waals (vdw) and Coulomb terms:

$$V_{sorbate} = V_{bond} + V_{bend} + V_{torsion} + V_{vdw} + V_{Coul}$$

Bond stretching and bending terms are modeled by harmonic potentials. The torsion potential is represented by a harmonic cosine function. The van der Waals interactions are described by a Lennard–Jones potential. The sorbate–sorbate and zeolite–sorbate interactions are described by Lennard–Jones plus Coulomb terms:

$$V_{Naphthalene-Naphthalene} = V_{Lennard-Jones} + V_{Coul}$$

Table 2
Analysis by energy dispersive X-ray spectroscopy (EDX) of NaX zeolite samples.

Samples	Elemental analysis by EDX							
	O	Na	Mg	Al	Si	K	Ca	Fe
Fresh zeolite	50.0	12.0	1.45	15.1	19.4	0.20	0.50	0.30

$$V_{\text{Zeolite–Naphthalene}} = V_{\text{Lennard–Jones}} + V_{\text{Coul}}$$

The parameters of the sorbate–sorbate and zeolite–sorbate interactions as well as the partial charges are reported in Supplementary materials described by [9,11,34]. The partial charges of sorbates were calculated according to DFT method at B3LYP/6-311++G(d,p) level of theory, after optimizing each electronic structure, by CHelpG method all performed by Gaussian 03 program [35]. The indication numbers of carbon and hydrogen atoms of naphthalene and anthracene molecules in order to use for partial charge calculation has been shown in Supplementary materials. For simplicity, some abbreviations are applied to indicate sorbate and zeolite atoms. Si, Al, O, and Na refer to the zeolite atoms and C_n and H_n are abbreviations applied for naphthalene and anthracene atoms and finally OC and CO refer to carbon dioxide.

4. Results and discussion

4.1. Thermal gravimetric analysis

Thermal gravimetric analysis (TGA) was carried out on a Mettler-Toledo (TGA/SDTA 851e). After loading, the samples of approximately 11.2754 mg were heated up to 800 °C, with a heating rate of 10 °C/min and at a flow air rate of 35 mL/min. The TGA profile and its derivative (DTG) for thermal decomposition of bi and tri aromatic compounds are shown in Fig. 3. There is one major decomposition peak located at 142.2 °C on DTG curve that corresponds to thermal decomposition of the contaminated compounds. The TGA/DTG profiles demonstrate that a temperature of approximately 400 °C is required for complete decomposition of contaminants.

However, critical conditions of naphthalene and anthracene (Table 3) are absolutely disparate of carbon dioxide; therefore, we can be ensured extraction process has not been touched by contaminants supercritical conditions.

4.2. Factorial design

Preliminary studies were performed in order to select relevant factors as well as their experimental domain to obtain the highest contaminant extraction recovery. Despite the fact that neat carbon dioxide may be sufficient to extract non-polar contaminants such as naphthalene and anthracene, two common modifiers, methanol (CH_3OH) and methylene chloride (CH_2Cl_2), were added to study the

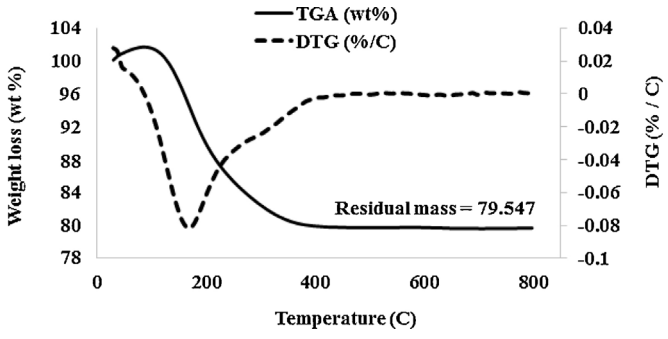

Fig. 3. TGA representation of weight loss of contaminated NaX zeolite sample.

Table 3
Some properties and critical conditions of naphthalene and anthracene.

Component	T_c (K)	P_c (bar)	ω	v_2^s
Naphthalene	748.4	40.5	0.302	0.111
Anthracene	869.1	30.8	0.353	0.143

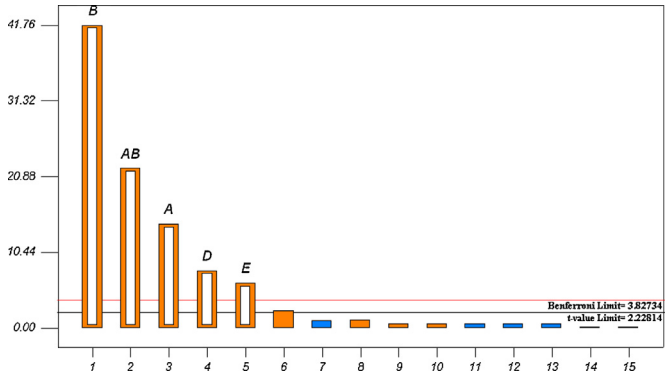

Fig. 4. Pareto chart of main effects obtained from 2^{5-1} fractional factorial designs. The vertical line defines the 95% confidence interval [A = T, B = P, D = CH_2Cl_2 and E = CH_3OH].

effect of the modifiers. The result was surprising; modifier addition did not show any considerable influence in comparison with pressure and temperature on contaminant recovery. Therefore, at the second part of experiments no modifier was added. Notice that extraction efficiency is defined as a ratio of the amount of the contaminants removed to the amount of the first sample mass.

Five factors were selected for the experimental design: pressure, temperature, time of extraction, and amount of modifiers (CH_3OH and CH_2Cl_2). A fractional two-level factorial design with five factors was then implemented; the range of these factors is reported in Table 4. In the experimental domain, extraction was carried out in the supercritical state. A two-level fractional factorial design (2^{5-1}) with an extra series of one variable test was performed in order to determine the main factors of the extraction process. Table 4 shows the experimental design and the results, which are derived from each run. The significance of the effects was checked by analysis of the variance (ANOVA) and Pareto chart (Fig. 4). The *P*-value shows the significance of the entire model and all parameters (<0.0001) except the factor time. The standardized effect of the independent variables and their interaction on the dependent variable was investigated by Pareto chart, which detects the main influence of the independent variables and interactions with their relative significance on the contaminants extraction. A positive value for the estimated effect indicates an increase in the extraction yield if the variable increases to its high level and a negative value indicates that a better extraction yield is obtained at low levels of the variables.

The interpretation of Pareto chart demonstrates that pressure and temperature are highly significant factors. An increase in pressure and temperature increases the contaminants extraction yield. The modifier is a matter of less significant specially methanol as a polar modifier for non-polar contaminants extraction. Time factor possesses an insignificant effect. The positive value for the effect of the pressure, temperature, and modifier volume indicate at the studied level, the extraction efficiency increases with increasing above factors. In conclusion, results of the fractional factorial design demonstrate that the variables (pressure and temperature) require a final optimization. Therefore, a one variable design was carried out.

In a system involving three significant independent variables T, P, and CH_2Cl_2 and CH_3OH modifiers, the mathematical relationship of the response on these variables can be approximated by a quadratic (second degree) polynomial equation as follow:

$$\begin{aligned}\text{Efficiency} = {} & 0.58097 - 2.42593 \times 10^{-3} \times T - 5.27778 \times 10^{-4} \times P \\ & + 0.023125 \times CH_2Cl_2 \\ & + 0.018125 \times CH_3OH + 1.90741 \times 10^{-5} \times P \times T\end{aligned} \quad (1)$$

Table 4
Experimental design the results obtained in function of the contaminated extracts yield (%).

Run no.	T (°C)	P (bar)	Density (g/cm^3)	Time (min)	CH_2Cl_2 (cm^3)	CH_3OH (cm^3)	Initial wt. (mg)	Initial coke wt. (mg)	Wt. change (mg)	Efficiency %
1	50	80	0.13	30	2	0	555.2	18.28	9.73	53.22
2	100	350	0.50	90	0	0	548.8	18.00	14.96	83.12
3	100	80	0.12	30	0	0	524.1	17.25	7.48	45.43
4	100	80	0.12	90	0	2	542.6	17.86	8.42	47.12
5	50	350	0.58	90	2	0	551.6	18.16	11.80	65.01
6	50	80	0.13	90	2	2	555.3	18.28	10.62	58.12
7	50	350	0.58	30	2	2	548.2	18.05	12.50	69.24
8	100	350	0.50	30	2	0	552.6	18.19	15.66	86.11
9	100	80	0.12	30	2	2	568.8	18.72	10.35	55.27
10	100	350	0.50	30	0	2	562.8	18.53	15.76	85.09
11	50	80	0.13	90	0	0	547.6	18.00	9.18	51.02
12	100	350	0.50	90	2	2	560.7	18.46	16.83	91.19
13	50	80	0.13	30	0	2	551.1	18.14	9.44	52.02
14	50	350	0.58	90	0	2	546.6	17.99	11.70	65.04
15	100	80	0.12	90	2	0	552.2	18.18	8.96	49.27
16	50	350	0.58	30	0	0	548.2	18.05	11.02	61.05

A multiple regression analysis was performed to obtain the coefficients and the equation, which can be used to estimate the response. It is important to note that all interactions higher than second order have been neglected in Eq. (1).

In this section, the experiments were conducted to find the optimum static extraction time, temperature and pressure of the supercritical extraction to efficiently activate the deactivated NaX zeolite. In this direction, the influence of different parameters including the extraction temperature (313.15–343.15 K) and pressure (100–200 bar), and static time (45–105 min) was investigated on the value of the extracted amount of the zeolite contaminants. The main point should be mentioned is that applied procedure to find the optimum operational conditions was obtained by the method of changing one factor at a time.

4.3. Effect of static extraction time

The time of extraction is expected to influence the extraction efficiency. The static mode expected a better penetration of the matrix by the fluid than the dynamic mode. So, in the second series of the experiments, the effects of static extractions periods on SFE efficiency of analytes were demonstrated. During the static extraction, the sample was allowed to steep in CO_2 fluid. Seven static extraction times (30, 45, 60, 75, 90, 105 and 120 min) were selected to find the optimum static time and to achieve the highest extraction amount of the NaX zeolite contaminations. Also, the pressure and temperature were fixed at 100 bar and 373.15 K. The obtained results showed that increasing the static extraction period from 30 to 90 min increases extraction efficiency of contaminants (Fig. 5). However, increasing the static extraction time from 90 to 120 min one may expect an increase in the extraction efficiency. However, since longer extraction times are not desirable and show a slight effect on the extracted amount of contaminates 90 min was considered as an optimum static extraction time.

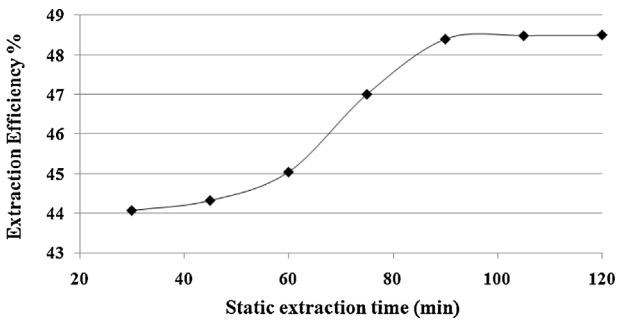

Fig. 5. The effect of static time on the amount of extraction of contamination from NaX zeolite.

4.4. Effects of pressure and temperature (density)

It has been well established that supercritical carbon dioxide solubility, a major factor responsible for extraction efficiency, can be changed by variation of density, viscosity, and diffusion characteristics of the supercritical fluid [20]. In other words, thermodynamic conditions of temperature and pressure (SCF density) are the main factors affecting SCE process. In the light of this fact, in the last part of this study, the effect of the extraction pressure and extraction temperature, while the other parameters including static extraction time were held constant, were investigated to study the efficiency of the contaminant extraction. Fig. 6 shows the effect of various temperatures (323.15, 343.15, and 373.15 K) and pressures (100, 200, 300, and 350 bar) on the extraction. In the first step, at the extraction temperature of 323.15 K different extraction pressures (100, 200, 300, and 350 bar) while the other parameters were fixed were examined on the amount of the extracted contaminates. The obtained results which are shown in Fig. 4 reveal that at the fixed extraction temperature of 323.15 K, an increase in the extraction pressure leads to an increase in the amount of the contaminates extraction. In other words, higher density caused by higher extraction pressure leads to the solubility strength of the supercritical carbon dioxide increase and enhances the amount of the solubilized contaminates. So, by increasing the extraction pressure higher amount of the contamination will be extracted from the samples. This observed trend was also repeated for the other isotherms of 343.15 and 373.15 K (Fig. 6). But, one can

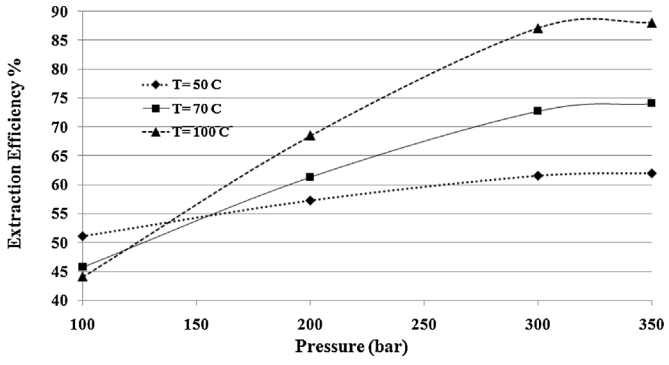

Fig. 6. The effect of the different extraction pressures and temperature on the amount of the extracted contaminates from the contaminated zeolite.

expect that an increase in the extraction temperature decreases the amount of the extracted values of contaminate. In the present study, an increase in the extraction temperature causes higher amount of extraction. This observed trend could be related to the fact that the extraction temperature has a two simultaneous effect on the solubility. The first effect is a decrease in the solubility of the substances in the supercritical condition due to lowering the density of the supercritical fluid. In other words, increasing the extraction temperature decreases the density of the supercritical fluid decreases the solubility strength of the substances. On the other hand, increasing the extraction temperature leads to increasing the solute vapor pressure that causes higher solubility of the substance in the supercritical fluid. The net effect of these two competing factors determined the reduction or increase of the substance solubility in the supercritical carbon dioxide. Based on the aforementioned statements, it seems that in the present study, the latter effect (solute vapor pressure) was dominant and leads to higher extraction of contaminates as the extraction temperature increases.

Besides its effect on solubility, temperature can affect rates of SFE through solute interactions with the matrix, as in kinetically controlles desorption of contaminants. Therefore, the total amount of solute that can be desorbed may sometimes depend on temperature alone and a higher temperature can increase recovery even at lower SCF density.

Moreover, it has been well documented that at low pressure, the higher the temperature leades to the lower density of supercritical fluid and solubility, and extraction efficiency as well. But, conversely, Brunner [36] and Palmer and Ting [37] reported that a rise in temperature, a minor decline in supercritical fluid density was shown at an elevated pressure, which in turn results in higher extraction efficiency probably because of an enhancement of the solute vapor pressure effect. These reported results show that the obtained results in the present study is in a good agreement with Brunner [36] and Palmer and Ting [37] findings. Furthermore, Araujo et al. [38] reported that, theoretically, the higher the pressure, the larger density and solubility the supercritical fluid, and better the extraction efficiency. However, a high pressure may also decrease supercritical fluid diffusivity leading to a lower extraction yield because of decreased interaction between supercritical fluid and sample. Thus, the diffusivity decrease should play a more important role in lowering yield of isoflavone at 400 bar than density increase. A similar outcome was reported by Macias-Sanchez et al. [39] who found a pressure of 500 bar to be lower in extraction yield of chlorophyll in microalga than 400 bar at the same temperature. Finally, based on these results and experiments, the optimum extraction pressure and temperature are proposed to be 350 bar and 373.15 K, respectively. The observed trends in Fig. 6 illustrate satisfactory agreement with the experimental trends of the solubility of naphthalene and anthracene in supercritical carbon dioxide computed using temperature-independent parameters in the new mixing rule for the PR EOS [40].

4.5. MD simulation results

Fig. 7 shows simulated snapshot of a typical configuration of naphthalene/CO_2 and anthracene/CO_2 molecules in one SC of FAU, respectively. The sorbate molecules prefer to accommodate parallel with respect to to the surface of SC. The planes of the aromatic rings are perpendicular with respect to FAU pore structure, frequently found in this zeolite at various loadings molecules/SC.

Mean square displacements (MSD) and the velocity auto correlation function (VACF) obtained from the simulations can be used

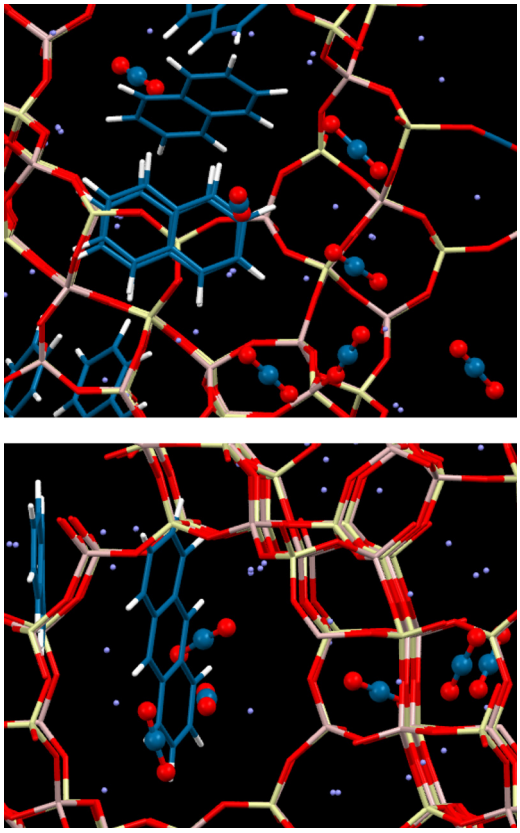

Fig. 7. Typical snapshotof naphthalene/CO_2 configuration at 298 K and 1 bar in zeolite-8 naphthalene-34 carbon dioxide (top) and zeolite-8 anthracene-34 carbon dioxide (bottom).

in analyzing the self-diffusion coefficients following the Einstein and Green-Kubo equations [41].

$$D = \frac{1}{6}\lim_{t\to\infty}\frac{\partial \mathrm{MSD}}{\partial t} = \frac{1}{6t}\left\langle \sum_{j=1}^{N_m}\left[r_j(t) - r_j(0)\right]^2 \right\rangle \tag{2}$$

$$D = \frac{1}{3N_m}\int_0^\infty \left\langle \sum_{j=1}^{N_m} v_j(t)\cdot v_j(0)\right\rangle \mathrm{d}t \tag{3}$$

where $r(t)$ and $v(t)$ are three-dimensional sorbate position and velocity at time t, respectively, and N_m is the component loading. Einstein and Green–Kubo relationships are equal in theory. The term $\left\langle \sum_{j=1}^{N_m}\left[r_j(t) - r_j(0)\right]^2 \right\rangle$ in Einstein relation is regarded as MSD, while the term $\left\langle \sum_{j=1}^{N_m} v_j(t)\cdot v_j(0)\right\rangle$ in Green–Kubo relation is usually called VACF. The values of the diffusion coefficients derived from the MSDs and VAFs are reported in Table 5 for sub and supercritical conditions.

We note that the diffusion coefficient evaluated at standard condition, temperature (298 K) and pressure (1 bar), for the zeolite-CO_2 system is in excellent agreement with the simulated value of 6.0×10^{-6} $cm^2\ s^{-1}$ and experimental value of 9.0×10^{-6} $cm^2\ s^{-1}$ measured by Quasi-Elastic Neutron Scattering (QENS) reported

Table 5
Calculated self-diffusion for CO_2 in NaX at sub and supercritical conditions for zeolite-8 naphthalene-34 CO_2 system.

P–T	Self-diffusivity ($cm^2\ s^{-1}$)
1 bar—298 K	6.31×10^{-6}
500 bar—373 K	1.11×10^{-5}

Table 6
Self-diffusion for CO_2 in NaX at 1 bar and various temperatures for zeolite-8 naphthalene-20 CO_2 system.

T (K)	Self-diffusivity ($cm^2\ s^{-1}$)
298	1.49×10^{-6}
373	1.86×10^{-6}
473	1.75×10^{-6}
573	1.61×10^{-6}

Table 7
Calculated self-diffusion for CO_2 in NaX at sub and supercritical conditions for zeolite-8 anthracene-34 CO_2 system.

P—T	Self-diffusivity ($cm^2\ s^{-1}$)
1 bar—298 K	8.81×10^{-7}
500 bar—373 K	1.12×10^{-6}

by Plant et al. [33]. This good agreement between experiment and simulation validates the present adjustment of the force-field parameters. A major feature of the data presented in Table 5 is that the calculated diffusion coefficient value in NaX at subcritical condition is lower in magnitude than that evaluated at the supercritical condition. This difference suggests that the confinement effect induced by the zeolite framework cannot decrease the self-diffusivity of the CO_2 molecules at higher temperatures and pressures. The calculated self-diffusion coefficient for lower loading CO_2 in zeolite-8 naphthalene-20 CO_2 system at 1 bar and various temperatures (298, 373, 473, and 573 K) has been shown in Table 6.

It can be seen from Table 6 that at constant pressure (1 bar) there is an increase in the diffusion coefficients for temperature increase from 298 to 373 K. That is, the diffusivity increases with increasing temperature. Thus, with each successive increase in temperature there is less available space for the fast moving of CO_2 molecules because of the existence of other large molecules such as naphthalene; hence, the movement becomes hindered. At higher temperatures, the molecules have the higher mobility but in the other hand there is more restricted area to move. It means at higher temperatures, we observe reduced translational mobility due to a reduced volume for the individual molecule. Generally, the diffusivity also decreases with increasing pressure and the sorbate–sorbate interaction further contributes to the decreased mobility with increasing pressure. But by passing the supercritical region self-diffusivity of CO_2 increases sharply and this can be contributed to two different aspects of CO_2 solubility at sub and supercritical conditions.

Calculated self-diffusion coefficients of CO_2 in zeolite-8 anthracene-34 CO_2 system are reported in Table 7. The self-diffusion coefficient of CO_2 in contaminated zeolites decreases with increasing the size of contaminants (anthracene against naphthalene) due to the steric hindrance ('friction') between sorbate molecules passing each other. This is not surprising, since an increased movement of CO_2 molecules will cause more accessibility of contaminant molecules by CO_2 as solvent and leads to more solubility. However, the diffusivity increases from sub to supercritical conditions.

Several studies on diffusion of light alkanes and single aromatics such as benzene in zeolites by Monte Carlo or MD simulations exist in the literature [9,10,13–15,22,31,42,43]. To the best of our knowledge, no experimental results for zeolite-naphthalene/anthracene-CO_2 self-diffusion in FAU have been reported. As a result, it can be found that the present results reveal new molecular insights for considering NaX confined polyaromatics solubility in supercritical CO_2.

Radial distribution functions (RDFs) analysis gives us insight information about positions and structural characteristics of sorbates in the pore of zeolites. Fig. 8 shows RDFs of CO_2 in zeolite pores (OC with zeolite atoms) at the temperature and pressure of 298 K and 1 bar (subcritical) and 373 K and 500 bar (supercritical) for system including 8 naphthalene and 34 CO_2.

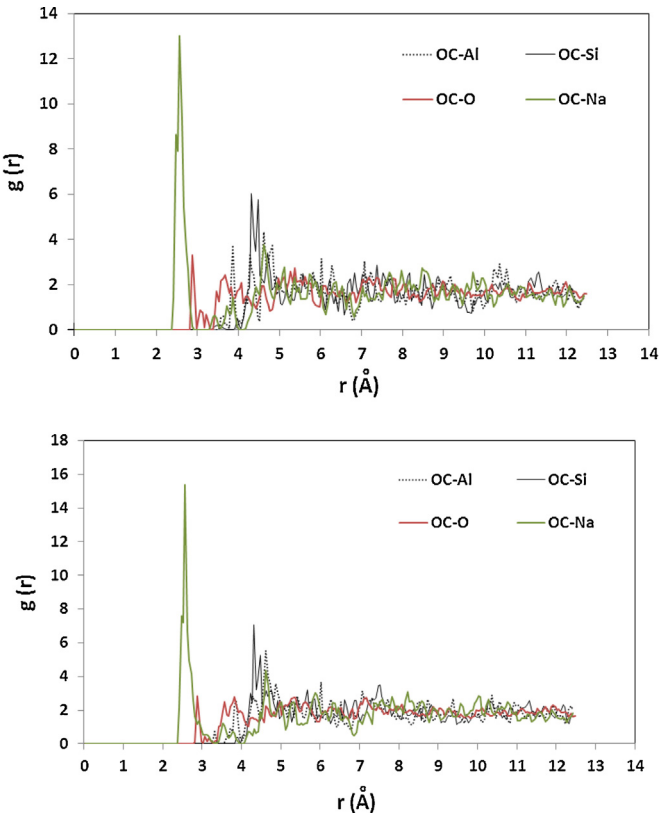

Fig. 8. Radial distribution function of the center of mass of carbon dioxide (OC) with zeolite atoms at subcritical (298 K and 1 bar, top) and supercritical conditions (373 K and 500 bar, bottom) for system zeolite-8 naphthalene-34 CO_2.

It is revealed from the first maximum peak of the cations surrounded by adsorbed molecules that the extraframework cations are the most preferable sites for CO_2 adsorption which is in qualitative agreement with the adsorption position of the same sorbates in NaY zeolite [44]. Whereas the height of OC–zeolite RDF increases at supercritical conditions, it is concluded that the probability of finding supercritical CO_2 in the vicinity of cation Na is higher than subcritical condition. The same position of RDF with changing conditions, 2.7 Å, besides the slight difference in height confirms carbon dioxide is adsorbed ideally to extraframework cations at the overall range of sub and supercritical conditions. For all loadings of sorbates in FAU, the first peak position does not experience any change and keeps its first peak at about 2.7 Å. A general point of view is that the height of the peak maximum in RDF increases with increasing temperature for zeolite-naphthalene-CO_2. It may be related to the rearrangement of adsorbed molecules in a parallel configuration as a function of temperature and steric hindrance. Similar configuration has been revealed for system zeolite-8 anthracene-34 CO_2.

Fig. 9 compares the RDFs of OC with naphthalene atoms (C and H) at sub and supercritical conditions, 298 K and 1 bar and 373 K and 500 bar. The most important point to mention is that the position of the first peak of g(r) OC—H is observed at 2.7 Å while the first peak of $g(r)_{OC-C}$ is located almost over 3.5 Å. This comparison reveals that the hydrogen atoms are the most preferable sites for carbon dioxide adsorption. Consequently, it can be concluded that hydrogen bonding would be one preferable mechanism to describe this phenomenon.

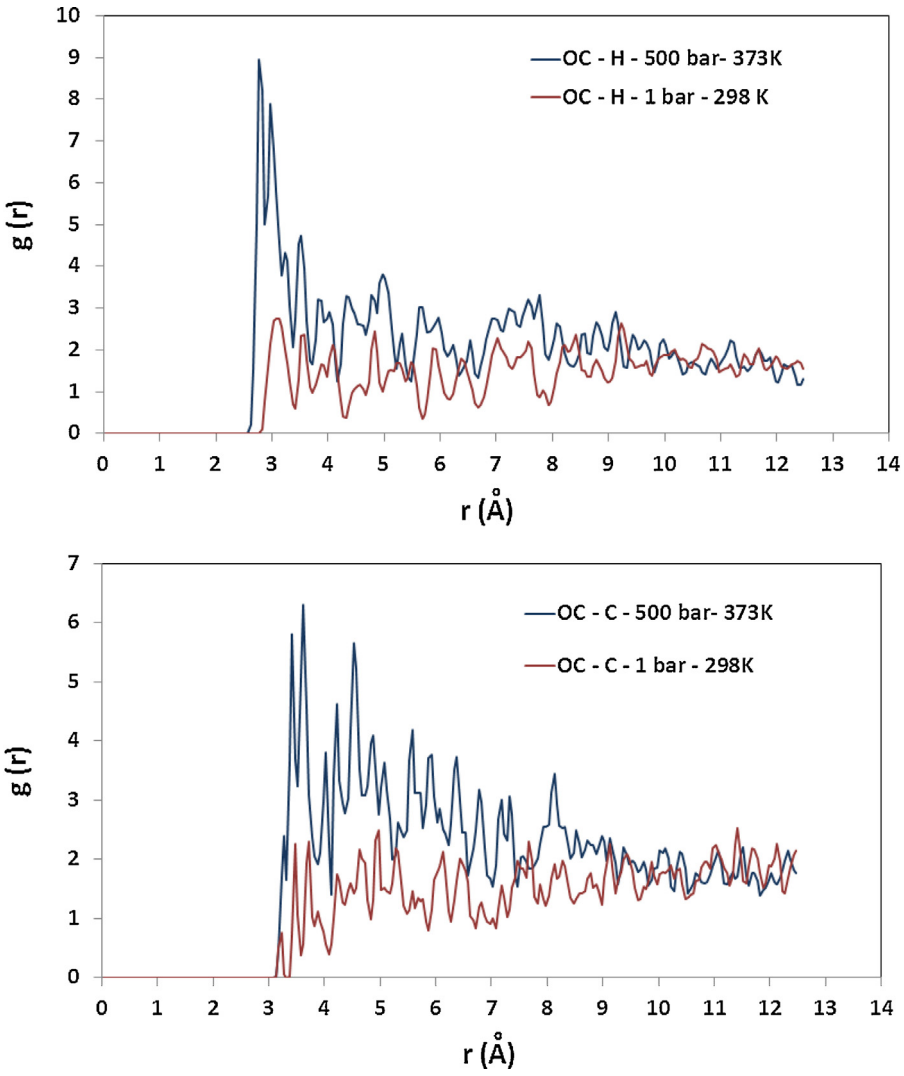

Fig. 9. Radial distribution function of the center of mass of carbon dioxide (OC) with C and H of naphthalene at subcritical (298 K and 1 bar, top) and supercritical conditions (373 K and 500 bar, bottom) for system zeolite-8 naphthalene-34 CO_2.

In order to investigate the effect of temperature and pressure on the removal process, it would be nice to consider the variation of sorbate–zeolite with these two important parameters. The position of the first peak and the height of RDF at two cases of sub and supercritical conditions reveal that the effect of pressure is more effective than the opposed influence of temperature. It means that in spite of shifting the position of the first peak due to the temperature to the higher distances, pressure has a stronger effect on SFE process (as mentioned in Section 2). In the case of adsorption process for anthracene molecules as shown in Fig. 10, the distance among OC—H is changes from 3.0 Å for subcritical condition, 1 bar and 298 K, to 3.2 Å for the case of supercritical condition, 500 bar and 373 K, although the distance between OC—C is about 3.5 Å for the case of sub and supercritical conditions.

Basically, RDF peaks of anthracene-CO_2 have been completely shifted towards greater distances for both cases of sub and supercritical conditions. Fig. 10 shows the RDF of the OC—H and OC—C for system zeolite-8 anthracene-34 CO_2 at 1 bar and 298 K and 500 bar and 373 K, respectively. It can be seen that the intensity of the first peak of g(r) is almost the same for two cases and is happened at about 3.1 Å, which indicates the vicinity of anthracene atoms becomes increasingly less occupied by CO_2 atoms. As Fig. 10 demonstrates, the main peaks stay almost at the same position over the entire sub to supercritical range. It can be discussed that at two conditions, the less aggregation of carbon dioxide-anthracene atom pairs occurs; consequently, the hydrogen bonding may not be observed for anthracene-CO_2 interaction. This behavior may be corresponded to the difference between size and adsorption energy of naphthalene and anthracene molecules according to their calculated parameters at B3LYP/6-311++G (d, p) level of theory for contaminants atoms. This observation for naphthalene and anthracene is in reasonable agreement with the results of solubility of naphthalene and anthracene in supercritical CO_2 [33].

In target FAU zeolite, in spite that small molecules have freedom to move in all directions from one SC to another cage (intercage), this is not the case for larger molecules such as naphthalene and anthracene. Due to smaller size, CO_2 molecules (34 molecules/UC) are able considerably to move inside one SC than anthracene and anthracene. Movement tendency of CO_2 molecules towards the center of phase space shows a higher diffusion for naphthalene molecules within the zeolite pores rather than anthracene molecules. It also can be found that the vicinity of carbon dioxide with naphthalene molecules is much more than anthracene and consequently might increase the probability of hydrogen bonding. This hydrogen bonding may be interpreted as higher naphthalene solubility in supercritical carbon dioxide rather than anthracene.

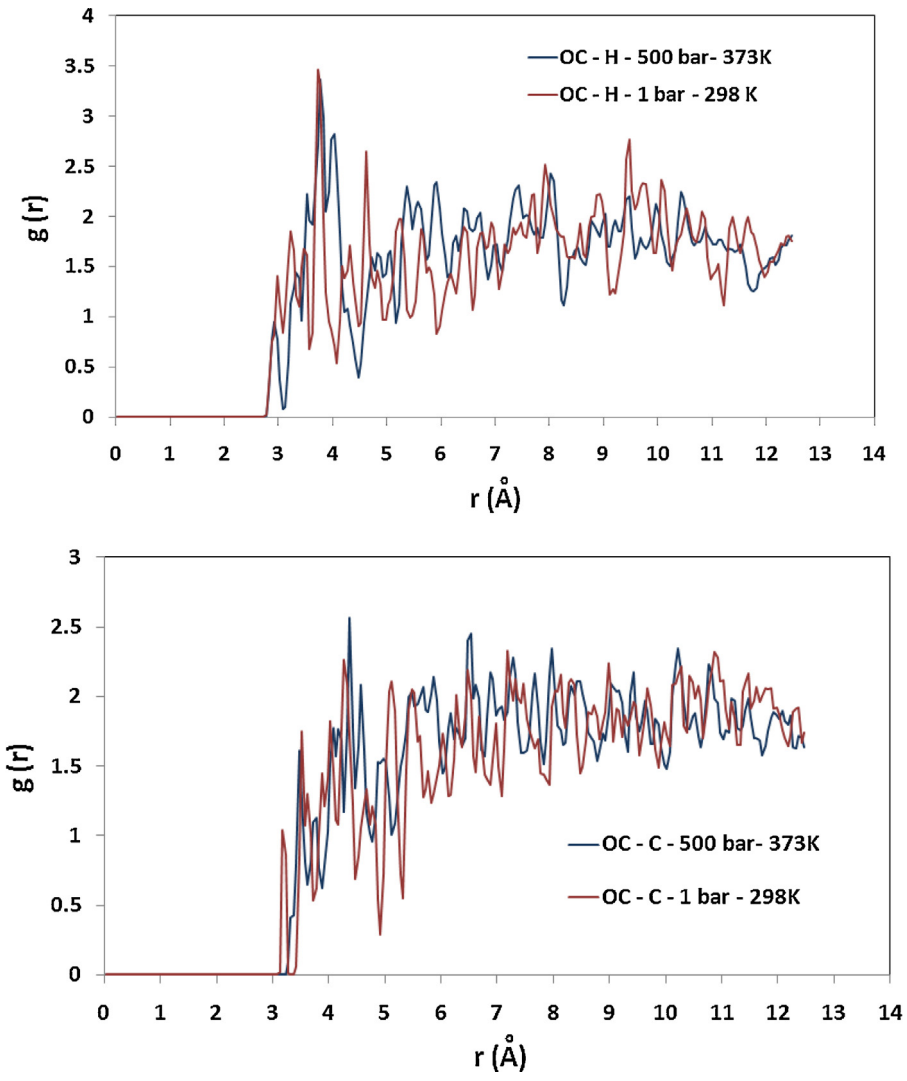

Fig. 10. Radial distribution function of the center of mass of carbon dioxide (OC) with C and H of anthracene at subcritical (298 K and 1 bar, top) and supercritical conditions (373 K and 500 bar, bottom) for system zeolite-8 naphthalene-34 CO_2.

We estimate finite-temperature adsorption energies of supercritical carbon dioxide with naphthalene and anthracene from energy minimizations. To see how, we begin with the molar adsorption energy, given by $\Delta U_{ads\,(G-C)} = \langle V_{(Z-G-C)}\rangle - [\langle V_{(Z)}\rangle + \langle V_{(Z-G)}\rangle + \langle V_{(Z-C)}\rangle]$, where $\langle V_{(Z-G-C)}\rangle$, $\langle V_{(Z)}\rangle$, $\langle V_{(Z-G)}\rangle$, and $\langle V_{(Z-C)}\rangle$ are the average potential energies of zeolite + guest + carbon dioxide, bare zeolite, zeolite + guest, and zeolite + carbon dioxide, respectively, all averaged in the canonical ensemble at temperature T. the calculated results were illustrated in Tables 8 and 9 for system zeolite–naphthalene–CO_2 and zeolite–anthracene–CO_2, respectively.

Table 8
Calculated adsorption energies for system zeolite-8 naphthalene-20 carbon dioxide at supercritical condition.

Adsorption energy (kcal/mol)	E_{cfg}	E_{vdw}	E_{cou}
E_{Z-G-CS}	-6.7301×10^4	1.6128×10^3	-6.9199×10^4
E_z	-6.6954×10^4	1.7412×10^3	-6.8696×10^4
E_{Z-G}	-6.7090×10^4	1.6495×10^3	-6.8874×10^4
E_{Z-C}	-6.7327×10^4	1.6126×10^3	-6.9088×10^4
E_{G-C}	13.4070×10^4	-3.3905×10^3	13.7459×10^4

Table 9
Calculated adsorption energies for system zeolite-8 anthracene-20 carbon dioxide at supercritical condition.

Adsorption energy (kcal/mol)	E_{cfg}	E_{vdw}	E_{cou}
E_{Z-G-C}	-6.7436×10^4	1.6693×10^3	-6.9286×10^4
E_z	-6.6954×10^4	1.7412×10^3	-6.8696×10^4
E_{Z-G}	-6.7204×10^4	1.6694×10^3	-6.9054×10^4
E_{Z-C}	-6.7327×10^4	1.6126×10^3	-6.9088×10^4
E_{G-C}	13.4049×10^4	-3.3539×10^3	13.7552×10^4

Tables 8 and 9 show the calculated Guest-CO_2 supercritical condition adsorption energies (E_{G-C}), for naphthalene and anthracene, respectively. From our MD simulations, the mean value of E_{G-C} shows an increase of 108 kcal/mol for anthracene adsorption in supercritical carbon dioxide. It might be interpreted that whereas the absorption of anthracene-supercritical carbon dioxide requires higher energies, lower solubility of anthracene molecules in supercritical carbon dioxide will occur.

5. Conclusions

Supercritical CO_2 is often promoted as a green solvent in green chemical separation process. Thus the SFE is one of the

prospective methods of zeolite regeneration. The application of this method might give an option to solve the problems of traditional regeneration methods. The results of SFE analysis by design experiment prove the removal of contaminating compounds from the microstructure NaX zeolite and support the possibility of application of SFE method for zeolite regeneration. The greater efficiency can be achieved by process parameters (T and P) adjustment. It is noted that the regenerability of NaX zeolite is not necessarily related to the extraction agent modification (particularly adding polar modifier).

In this study, a possible alternative SFE method could be modeled by the MD simulation. Radial distribution function of carbon dioxide with contaminated NaX zeolite by naphthalene and anthracene were under consideration. It is observed that extra framework cations as active sites demonstrate high occupation probabilities. It has been concluded that these extra framework cations are the most preferable sites for zeolite reactivation. It is noted that the calculated self-diffusion coefficients at various temperatures and pressures are almost in the range of 10^{-6} cm^2 s^{-1} which is in the range of experimental values. Strongest adsorption sites in NaX (extra framework cations) are well separated; as a consequence, stabilizing interactions between naphthalene and CO_2 molecules are strong and observed relative strong hydrogen bond which has been concluded as one of the major causes of SFE performance. This leads to the observed increase of the bi aromatic adsorption on supercritical conditions. We also estimate finite-temperature adsorption energies of supercritical carbon dioxide with naphthalene and anthracene from energy minimizations. Calculated adsorption energies show an increase of approximately 108 kcal/mol for anthracene adsorption in supercritical carbon dioxide. It might be interpreted as higher energy required for anthracene to be absorbed and consequently lower solubility by supercritical carbon dioxide. Generally, pair correlations as well as adsorption energies can be interpreted as higher naphthalene solubility in supercritical carbon dioxide rather than anthracene.

Acknowledgments

We gratefully acknowledge support from the High Performance Computing Centre of Ferdowsi University of Mashhad.

Appendix A. Supplementary data

Supplementary data associated with this article can be found, in the online version, at http://dx.doi.org/10.1016/j.supflu.2016.01.003.

References

[1] H. Deng, H. Yi, X. Tang, Q. Yu, P. Ning, L. Yang, Adsorption equilibrium for sulfur dioxide, nitric oxide, carbon dioxide, nitrogen on 13X and 5A zeolites, Chem. Eng. J. 188 (2012) 77–85.
[2] Y. Nakasaka, T. Tago, H. Konno, A. Okabe, T. Masud, Kinetic study for burning regeneration of coked MFI-type zeolite and numerical modeling for regeneration process in a fixed-bed reactor, Chem. Eng. J. 207–208 (2012) 368–376.
[3] P.A. Russo, M.M.L.R. Carrott, P.J.M. Carrott, P. Matias, J.M. Lopes, M. Guisnet, F.R. Ribeiro, Characterisation by adsorption of various organic vapours of the porosity of fresh and coked H-MCM-22 zeolites, Microporous Mesoporous Mater. 118 (2009) 473–479.
[4] G. Weber, J.P. Bellat, F. Benoit, C. Paulin, Adsorption equilibrium of light mercaptans on faujasites, Adsorption 11 (2005) 183–188.
[5] G. Weber, F. Benoit, J.-P. Bellat, C. Paulin, P. Mougin, M. Thomas, Selective adsorption of ethyl mercaptan on NaX zeolite, Microporous Mesoporous Mater. 109 (2008) 184–192.
[6] H. Yi, H. Deng, X. Tang, Q. Yu, X. Zhou, H. Liu, Adsorption equilibrium and kinetics for SO_2, NO, CO_2 on zeolites FAU and LTA, J. Hazard. Mater. 203–204 (2012) 111–117.
[7] J. Cejka, H.v. Bekkum, A. Corma, F. Schüth, Introduction to Zeolite Science and Practice, Elsevier, Amsterdam, 2007.
[8] M. Trejda, M. Ziolek, P. Decyk, D. Duczmal, The radical species and impurities present in mesoporous silicas as oxidation active centres, Microporous Mesoporous Mater. 120 (2009) 214–220.
[9] R. Rungsirisakun, T. Nanok, M. Probst, J. Limtrakul, Adsorption and diffusion of benzene in the nanoporous catalysts FAU, ZSM-5 and MCM-22: a molecular dynamics study, J. Mol. Graphics Modell. 2 (2006) 373–382.
[10] P. Wongthong, R. Rungsirisakun, M. Probst, J. Limtrakul, Adsorption and diffusion of light alkanes on nanoporous faujasite catalysts investigated by molecular dynamics simulations, Microporous Mesoporous Mater. 100 (2007) 160–166.
[11] A.M. Granato, N.L. Thijs, J.H. Vlugt, A.E. Rodrigues, Adsorption equilibrium of isobutane and 1-butene in zeolite 13X by molecular simulation, Ind. Eng. Chem. Res. 47 (2008) 6166–6174.
[12] Z. Yongping, J. Shengui, X. Weihong, C. Changlin, Adsorption of mercaptan from model gasoline on 13X loaded with Zn^{2+}, Can. J. Chem. Eng. 86 (2008) 186–191.
[13] T. Mosell, G. Schrimpf, J. Brickmann, Diffusion of aromatic molecules in zeolite NaY. 1. Constrained reaction coordinate dynamics, J. Phys. Chem. B 101 (1997) 9476–9484.
[14] D. Plant, H. Jobic, P. Llewellyn, G. Maurin, Diffusion of CO2 in NaY and NaX Faujasite systems: quasi-elastic neutron scattering experiments and molecular dynamics simulations, Eur. Phys. J.—Spec. Top. 141 (2007) 127–132.
[15] M.A. Granato, M. Jorge, T.H. Vlugt, A.E. Rodrigues, Diffusion of propane, propylene and isobutane in 13X zeolite by molecular dynamics, Chem. Eng. Sci. 65 (2010) 2656–2663.
[16] C. Laborde-Boutet, G. Joly, A. Nicolaos, M. Thomas, P. Magnoux, Selectivity of thiophene/toluene competitive adsorptions onto NaY and NaX zeolites, Ind. Eng. Chem. Res. 45 (2006) 6758–6764.
[17] S. Buttefey, A. Boutin, C. Mellot-Draznieks, A.H. Fuchs, A simple model for predicting the Na+ distribution in anhydrous NaY and NaX zeolites, J. Phys. Chem. B 105 (2001) 9569–9575.
[18] J. Zhang, N. Burke, S. Zhang, K. Liu, M. Pervukhina, Thermodynamic analysis of molecular simulations of CO_2 and CH_4 adsorption in FAU zeolites, Chem. Eng. Sci. 113 (2014) 54–61.
[19] H. Rajaei, A. Amin, A. Golchehre, F. Esmaeilzadeh, Investigation on the effect of different supercritical fluid extraction process on the activation of the R-134 catalyst, J. Supercrit. Fluids 67 (2012) 1–6.
[20] J.M. Becnel, K.M. Dooley, Supercritical fluid extraction of polycyclic aromatic hydrocarbon mixtures from contaminated soils, Ind. Eng. Chem. Res. 37 (1998) 584–594.
[21] D.C. Rapaport, The Art of Molecular Dynamics Simulation, Cambridge University Press, New York, 2004.
[22] P. Demontis, E.S. Fois, G.B. Suffritti, S. Quartieri, Molecular dynamics studies on zeolites. 4. Diffusion of methane in silicalite, J. Phys. Chem. B 94 (1990) 4329–4334.
[23] R.L. June, A.T. Bell, D.N. Theodorou, Molecular dynamics studies of butane and hexane in silicalite, J. Phys. Chem. 96 (1992) 1051–1060.
[24] H. Klein, H. Fuess, Mobility of aromatic molecules in zeolite NaY by molecular dynamics simulation, J. Phys. Chem. B 100 (1996) 11101–11112.
[25] I. Daems, P. Leflaive, A. Méthivier, J.F.M. Denayer, G.V. Baron, Size and packing related adsorption effects in the liquid phase adsorption of aromatics and alkenes on FAU type zeolites, Stud. Surf. Sci. Catal. 158 (2005) 1177–1184.
[26] H. Zheng, L. Zhao, J. Ji, J. Gao, C. Xu, F. Luck, Unraveling the adsorption mechanism of mono-and diaromatics in faujasite zeolite, ACS Appl. Mater. Interf. 7 (2015) 10190–10200.
[27] P. Lanteíri, R. Longeray, Chimiomeítrie: le mariage reíussi entre les sciences analytiques et l'informatique, Analusis 24 (1996) M17–M27.
[28] M. Haghighiasl, J. Sargolzaei, F. Moosavi, Identification of the coke deposited on 13X industrial zeolite molecular sieves during mercaptan removal process, Asia Pac. J. Chem. Eng. (2015), http://dx.doi.org/10.1002/apj.1952.
[29] F. Porcher, M. Souhassou, Y. Dusausoy, C. Lecomte, The crystal structure of a low-silica dehydrated NaX zeolite, Eur. J. Mineral. 11 (1999) 333–343.
[30] W. Smith, T.R. Forester, DL_POLY_2.0: a general-purpose parallel molecular dynamics simulation package, J. Mol. Graphics 14 (1996) 136–141.
[31] H. Ramanan, S.M. Auerbach, M. Tsapatsis, Beyond lattice models of activated transport in zeolites: high-temperature molecular dynamics of self-diffusion and cooperative diffusion of benzene in NaX, J. Phys. Chem. B 108 (2004) 17171–17178.
[32] P. Cosoli, M. Ferrone, S. Pricl, M. Fermeglia, Hydrogen sulfide removal from biogas by zeolite adsorption. Part II. MD simulations, Chem. Eng. J. 145 (2008) 93–99.
[33] D. Plant, H. Jobic, P. Llewellyn, G. Maurin, Diffusion of CO_2 in NaY and NaX faujasite systems: quasi-elastic neutron scattering experiments and molecular dynamics simulations, Eur. Phys. J. Spec. Top. 141 (2007) 127–132.
[34] W.D. Cornell, P. Cieplak, C.I. Bayly, I.R. Gould, K.M. Merz, D.M. Ferguson, D.C. Spellmeyer, Fox Thomas, J.W. Caldwell, P.A. Kollman, A second generation force field for the simulation of proteins, nucleic acids, and organic molecules, J. Am. Chem. Soc. 117 (1995) 5179–5197.
[35] M.J. F, G.W. T, H.B. S, G.E. S, M.A. R, J.R. C, J.A. M.J, T. V, K.N. K, J.C. B, M. J.M, Gaussian 03, Revision A. 1, Gaussian. Inc, Pittsburgh, PA, 2003.
[36] G. Brunner, Supercritical fluids: technology and application to food processing, J. Food Eng. 67 (2005) 21–33.
[37] M.V. Palmer, S.S.T. Ting, Applications for supercritical fluid technology in food processing, Food Chem. 52 (1995) 345–352.

[38] J.M.A. Araujo, M.V. Silva, J.B.P. Chaves, Supercritical fluid extraction of daidzein and genistein isoflavones from soybean hypocotyls after hydrolysis with endogenous B-glucosidases, Food Chem. 105 (2007) 266–272.
[39] M.D. Macias-Sanchez, C. Mantell, M. Rodriguez, E.M.d.l. Ossa, L.M. Lubian, O. Montero, Supercritical fluid extraction of carotenoids and chlorophyll a from *Nannochloropsis* gaditana, J. Food Eng. 66 (2005) 245–251.
[40] F. Esmaeilzadeh, H. As'adi, M. Lashkarbolooki, Calculation of the solid solubilities in supercritical carbon dioxide using a new Gex mixing rule, J. Supercrit. Fluids 51 (2009) 148–158.
[41] L.W. Zhong, C. Cong, Y. Jian, Molecular dynamics simulation of self-diffusion coefficient and its relation with temperature using simple Lennard-Jones potential, Heat Transfer—Asian Res. 37 (2008) 86–93.
[42] E. Beerdsen, D. Dubbeldam, B. Smit, Loading dependence of the diffusion coefficient of methane in nanoporous materials, J. Phys. Chem. B 110 (2006) 22754–22772.
[43] D.F. Plant, G. Maurin, R.G. Bell, Diffusion of methanol in zeolite NaY: a molecular dynamics study, J. Phys. Chem. B 111 (2007) 2836–2844.
[44] C. Baehtz, H. Fuess, Naphthalene, anthracene and 2,3-benzanthracene in zeolite Y, Phys. Chem. Chem. Phys. 4 (2002) 4543–4548.